Journal of Radioanalytical and Nuclear Chemistry (2021) 328:195–203
https://doi.org/10.1007/s10967-021-07639-6

Chlorination technique for decontamination of radioactive concrete waste contaminated by Sr

Min Ku Jeon[1,2] · Sung-Wook Kim[1] · Keun-Young Lee[1] · Maeng-Kyo Oh[1,3]

Received: 4 November 2020 / Accepted: 9 February 2021 / Published online: 25 February 2021

Abstract
The feasibility of the chlorination reaction as a decontamination technique for ^{90}Sr-contaminated concrete waste was investigated via thermodynamic and experimental approaches. Thermodynamic calculations suggested that SrO reacts with chlorine prior to CaO, $CaCO_3$, and MgO, while other oxides remain in their oxide forms. It was found experimentally that a temperature of at least 700 °C is required to convert more than 40% of SrO into $SrCl_2$. A set of comparison experiments performed at various temperatures verified that CaO exhibits higher conversion ratios than those of SrO, while significantly lower ratios were observed with $CaCO_3$.

Keywords Strontium-90 · Chlorination reaction · Concrete waste · Decontamination · Decommissioning

Introduction

During the decontamination and decommissioning of nuclear power plants (NPPs), radioactive ^{90}Sr is of serious concern owing to its high mobility and long half-life of 28.8 years [1]. In addition, ^{90}Sr behaves like Ca in the human body, and it accumulates in the bones and teeth, resulting in associated cancers [2]. ^{90}Sr is known as a common contaminant of structural materials of NPPs [3] and also observed in NPP accidental sites such as the Chernobyl and Fukushima Daiichi sites [4]. Recently, the government of the Republic of Korea announced the termination of the operation of the Kori-1 (pressurized light water reactor) and Wolsung-1 (Canadian deuterium reactor) NPPs, and decommissioning plans are underway including challenging tasks to be demonstrated before being adopted in the field.

✉ Min Ku Jeon
minku@kaeri.re.kr

[1] Korea Atomic Energy Research Institute, 111, Daedeok-daero 989, Yuseong-gu, Daejeon 34057, Republic of Korea

[2] Department of Quantum Energy Chemical Engineering, University of Science and Technology, 217, Gajeong-ro, Yuseong-gu, Daejeon 34113, Republic of Korea

[3] Department of Chemical and Biomolecular Engineering, Yonsei University, 50 Yonsei-ro, Seodaemun-gu, Seoul 03722, Republic of Korea

In this work, we focus on decontaminating ^{90}Sr-contaminated concrete waste. Concrete is normally composed of an aggregate matrix (60–75%) and a binder (25–40%) which holds the matrix materials together. The aggregate matrix is a mixture of fine materials (such as sand) and coarse ingredients (such as gravel or crushed rocks). SiO_2 is known to be the main constituent of these materials, with Al_2O_3 the second most abundant component. Various oxides such as Na_2O, MgO, SO_3, K_2O, CaO, and Fe_2O_3 are also present in the aggregate matrix as minor constituents [5]. Portland cement is the most widely used binder, consisting of CaO (~63%), SiO_2 (~22%), Al_2O_3 (~7%), and minor amounts of Fe_2O_3, MgO, and SO_3 [6]. Adding water to the binder induces a hydration reaction, producing cement paste that glues the matrix constituents together.

Currently, decontamination techniques for concrete waste can be categorized into mechanical and chemical techniques [7]. The key idea of mechanical techniques is that the contamination is concentrated at the surface of the concrete waste. Thus, various mechanical surface-exfoliating techniques are employed for materials in this category [8]. The chemical technique employs various mineral and organic acids, surfactants, gels, and foam chemicals for the dissolution of radioactive waste with or without non-radioactive concrete itself. These wet chemical techniques can achieve higher decontamination factors than mechanical techniques, though the generation of secondary waste remains as a critical issue. A brand new approach that employs chlorine gas

as a selective reaction medium for the decontamination of ^{90}Sr-contaminated concrete waste is introduced in this study. Some metal oxides are reactive with chlorine gas without the support of a reducing agent such as carbon. Normally, metal chlorides have considerable solubility in water and higher volatility than their oxide forms. The key idea of this chlorination decontamination technique is the selective conversion of radioactive contaminants into their chloride forms so that they can be separated via water washing or a heat treatment (i.e., distillation). Among the various constituents of concrete waste, a couple of experimental results related to chlorination reactions of CaO [9] and $CaCO_3$ [10] have been found. Yake and Ulrichson investigated the chlorination reaction behavior of CaO at 333–472 °C, and the formation of $CaCl_2$ was confirmed [9]. The reaction between $CaCO_3$ and Cl_2 was demonstrated by Orosco et al. [10] using a thermogravimetric analysis technique, indicating that the chlorination reaction occurred at 420–900 °C. However, there are no experimental data available for SrO. In the present study, theoretical and experimental approaches were conducted in order to investigate the feasibility of the chlorination decontamination technique for application to the decontamination of ^{90}Sr-contaminated concrete waste.

Experimental

Theoretical calculations were conducted using the "Reaction Equations" and "Equilibrium Compositions" modules of HSC chemistry 9.5.1 [11]. The Reaction Equations module was utilized to calculate the Gibbs free energy change (ΔG) and equilibrium constant (K) values for various reaction equations of the representative species in concrete waste in the temperature range of 0–1000 °C. The Equilibrium Compositions module was utilized for a quantitative analysis of the chlorination reaction behavior of SrO in the presence of CaO, $CaCO_3$, or MgO. These calculations were performed at various reaction temperatures (200–1000 °C) and chlorine input. The initial amount of chlorine input was set to 1/10 of SrO and was then increased to 100 times the initial amount (= 10 times the initial amount of SrO). Idential calculations were also repeated for $SrCO_3$ instead of SrO. The input data for the calculations are listed in Table 1. During the calculations, the pressure of the system was set to 1.0 bar.

Chlorination experiments were conducted using a horizontal quartz tube reactor with a diameter of 4 cm. On the inlet side, the reactor was connected to a gas feed system which separately controls the flow rates of argon and chlorine gases using mass flow controllers (MFCs, Kofloc co., Japan, Model 3660 for Ar and 5440 for Cl_2). In the middle of the reactor, a heater was positioned to control the reaction temperature. Schematic diagram of the reaction system is shown in Fig. 1. As it is known that SrO reacts with CO_2 in the air to form $SrCO_3$, SrO powder (Sigma-Aldrich, 99.9%) was heat treated at 800 °C for 4 h under a 200 mL/min O_2 flow before chlorination experiments. Approximately 1.20 g of heat treated SrO was employed for each chlorination experiment. The samples were loaded in an alumina boat and then placed in the middle of the quartz reactor. After purging the reactor with an argon gas flow, the heater began to heat the reactor to the target temperature at a ramping rate of 10 °C/min. After the heater temperature was stabilized

Table 1 Input data for calculations of equilibrium composition using the HSC chemistry software

Input data for	Reactant 1	Reactant 2	Initial Cl_2 amount (mmol)	Final Cl_2 amount (mmol)
Figure 2a, b	CaO 1.00 kmol	SrO 1.00 mmol	0.100	10.0
Figure 2c, d	$CaCO_3$ 1.00 kmol	SrO 1.00 mmol	0.100	10.0
Figure 2e, f	MgO 1.00 kmol	SrO 1.00 mmol	0.100	10.0
Figure 3a, b	CaO 1.00 kmol	$SrCO_3$ 1.00 mmol	0.100	10.0
Figure 3c, d	$CaCO_3$ 1.00 kmol	$SrCO_3$ 1.00 mmol	0.100	10.0
Figure 3e, f	MgO 1.00 kmol	$SrCO_3$ 1.00 mmol	0.100	10.0

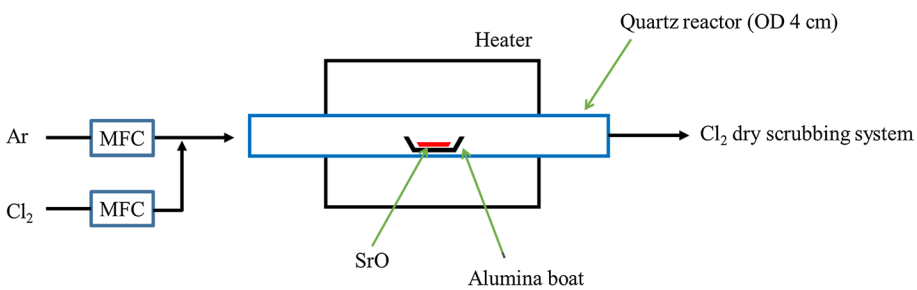

Fig. 1 Schematic diagram of the experimental set-up

at the reaction temperature, the gas flow rate was changed from 150 mL/min Ar to 96 mL/min Ar + 4 mL/min Cl_2 and maintained during the reaction. The effects of the reaction time and temperature were investigated for SrO by repeating the abovementioned process. The chlorination experiments were also conducted using CaO (Sigma-Aldrich, 99.9%, powder), $CaCO_3$ (Sigma-Aldrich, > 99.0%, powder), and $SrCO_3$ (Sigma-Aldrich, > 98%, powder) as a function of the reaction temperature in order to compare the corresponding chlorination reaction characteristics with those of SrO.

Phase changes of the reacted samples were analyzed using an X-ray diffraction system (XRD, Bruker D8 Advance). The XRD signals were measured in the 2θ range of 10–80° with a step size of 0.0104° and measurement time of 0.15 s during each step.

Results and discussion

Calculating the ΔG value of a reaction is the first step when estimating the feasibility of a reaction under a certain condition. Figure 2a shows the ΔG calculation results for chlorination reactions of the various oxides that make up the major constituents of the aggregate matrix. A positive value of ΔG indicates that the reaction products have higher chemical potential than the reactants and that the reaction will not likely proceed toward the right-hand direction. On the other hand, a negative ΔG value indicates that the reaction is thermodynamically feasible to generate reaction products. Among the reactions considered in this work, it is clear that Al_2O_3, SiO_2, and Fe_2O_3 are not reactive with chlorine up to 1000 °C. MgO exhibited mixed values, mostly negative except in the temperature range of 465–714 °C. Figure 2b displays the ΔG calculation results for chlorination reactions of various oxides and carbonates of Ca and Sr. Calcium compounds, CaO, $CaCO_3$, and $Ca(OH)_2$, showed negative ΔG values in the entire temperature range matching those of Sr compounds. It is important to note that various chemical forms of Ca were considered here, as CaO, the initial form as an ingredient of concrete, reacts with water to produce $Ca(OH)_2$ and then is slowly converted into $CaCO_3$ by reacting with CO_2 in air. The calculations for $Ca(OH)_2$ were conducted only up to 400 °C as it decomposes at 396–481 °C [12]. According to the ΔG values, the thermodynamic preference for the chlorination reaction was CaO > ($Ca(OH)_2$) > $CaCO_3$ in the entire temperature range. For Sr, SrO is known as the major chemical form in used oxide fuels [13]. However, it can react with water or CO_2 to produce $Sr(OH)_2$ or $SrCO_3$, respectively, after being exposed to air. The calculations for $Sr(OH)_2$ were limited to 500 °C as it decomposes in the tempearture range of 475–575 °C [12], and it was found that $Sr(OH)_2$ exhibits higher ΔG values than those of SrO. The calculations for $SrCO_3$ and $CaCO_3$ were limited to 700 °C for the same reason described above [14, 15]. Among the three Sr compounds, SrO exhibited the lowest ΔG value in the entire temperature range. These calculation results suggest that, along with Sr compounds, Ca compounds and MgO may also be converted to $CaCl_2$ and $MgCl_2$, respectively, during the chlorination reaction.

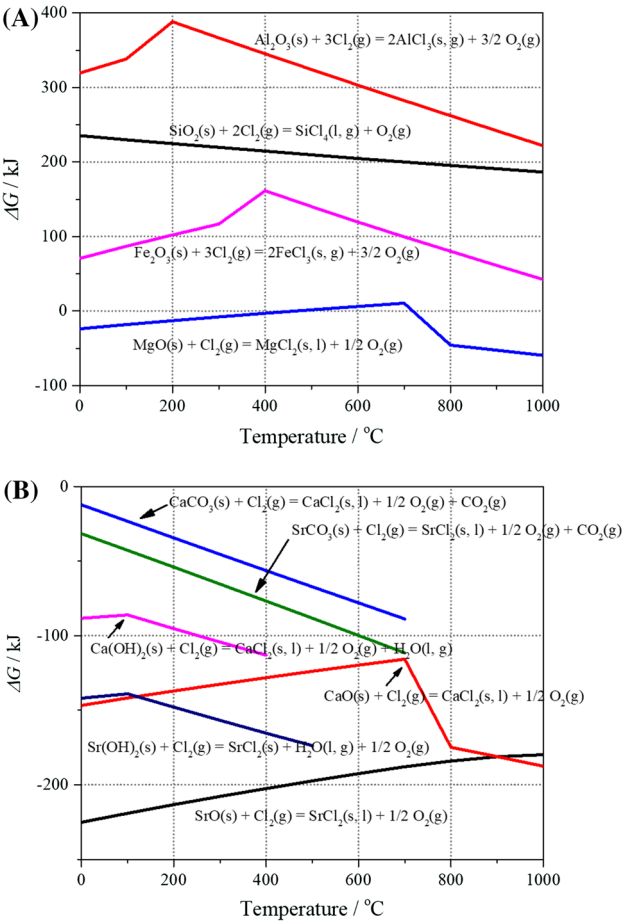

Fig. 2 Gibbs free energy change (ΔG) values of **a** Al_2O_3, SiO_2, Fe_2O_3, and MgO and **b** $CaCO_3$, CaO, $Ca(OH)_2$, SrO, $Sr(OH)_2$, and $SrCO_3$ for the chlorination reaction in the temperature range of 0–1000 °C calculated using the HSC chemistry code

A quantitative analysis was conducted using the Equilibrium Compositions module to predict the chlorination reaction behaviors of SrO and $SrCO_3$ in the presence of CaO, $CaCO_3$, or MgO, which were identified as being reactive with chlorine in the ΔG calculations. The quantitative analysis results are shown in Fig. 3 as functions of the reaction temperature (200–1000 °C) and the input amount of Cl_2. As an indicator of conversion selectivity for SrO and $SrCO_3$, the ratio of $SrCl_2$ to $CaCl_2$ or $MgCl_2$ in an equilibrium state is employed. Figure 3a shows the effects of the reaction temperature and the input amount of Cl_2 on the SrO–CaO system with an initial SrO concentration of 1 ppm versus CaO. It is clear in the figure that an increase in the reaction

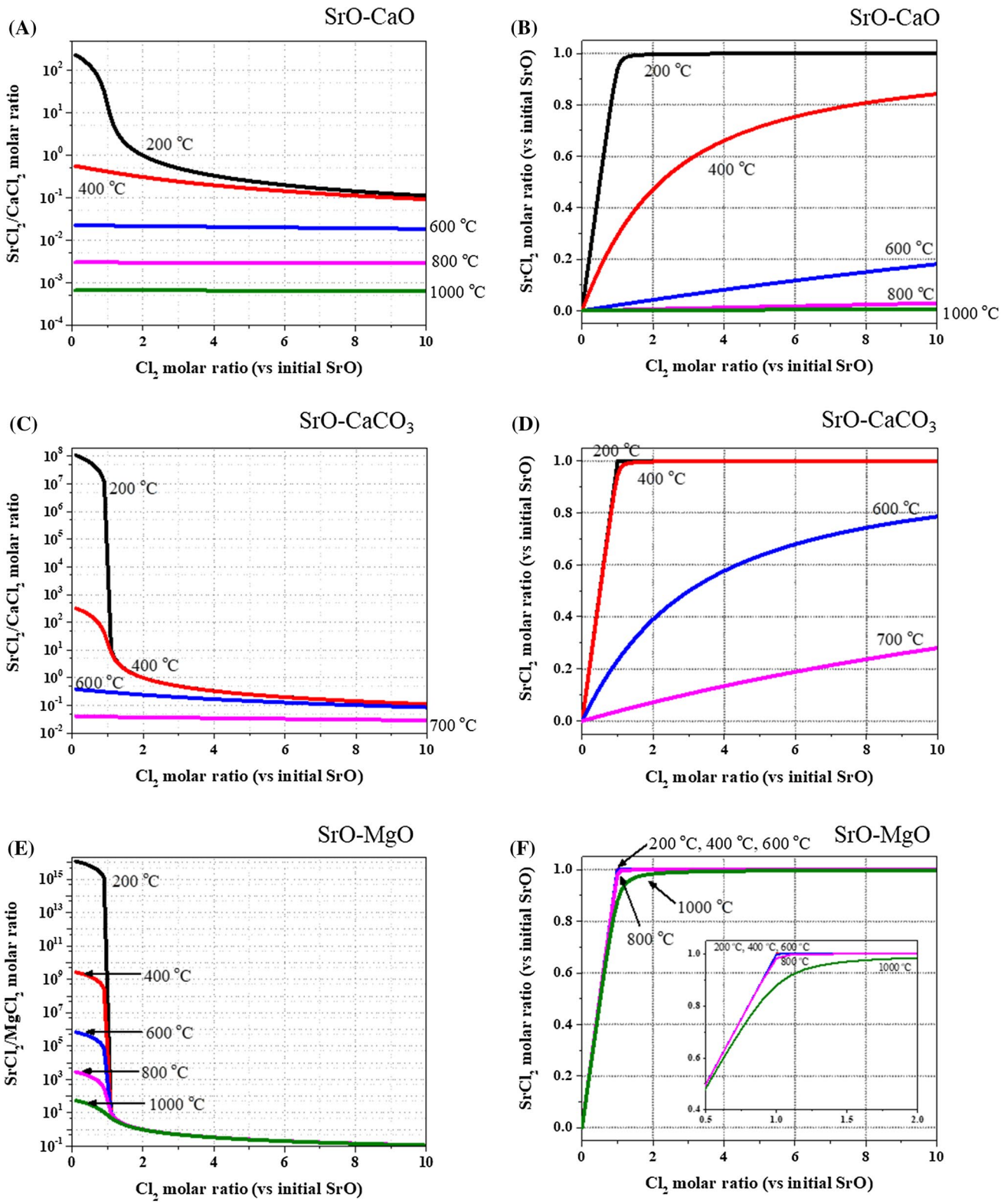

Fig. 3 Equilibrium compositions (**a**, **c**, **e**) and conversion ratios of $SrCl_2$ (**b**, **d**, **f**) for the SrO–CaO (**a**, **b**), SrO–$CaCO_3$ (**c**, **d**), and SrO–MgO (**e**, **f**) systems at various temperatures and Cl_2 molar ratios with an initial SrO concentration of 1 ppm versus CaO, $CaCO_3$, or MgO

temperature results in a decrease in the $SrCl_2/CaCl_2$ ratio due to the chlorination reaction of CaO. Figure 3b shows the ratio of $SrCl_2$ over the initial amount of SrO, in which it is clear that an increase in the reaction temperature leads to a decrease in the $SrCl_2$ ratio. This result indicates that the CaO chlorination reaction is preferred over the SrO chlorination reaction at temperatures greater than 400 °C. In the SrO–$CaCO_3$ system shown in Fig. 3c, d, especially high $SrCl_2/CaCl_2$ values were observed at 200 and 400 °C when the Cl_2 molar ratio was smaller than 1. In addition, the $SrCl_2/CaCl_2$ ratio increased from 0.0184 in the SrO–CaO case to 0.0853 in the SrO–$CaCO_3$ case at 600 °C and at Cl_2 molar ratio of 10. These results indicate that the selective conversion of SrO is more convenient in the SrO–$CaCO_3$ system compared to the SrO–CaO system because the chlorination reaction of $CaCO_3$ occurs at higher temperatures than that of CaO. The calculations for the SrO–$CaCO_3$ were conducted up to 700 °C due to the thermal decomposition of $CaCO_3$ into CaO and CO_2 above 700 °C [15]. With regard to MgO, as shown in Fig. 3e, f, the $SrCl_2/MgCl_2$ ratios exceeded 0.111 regardless of the reaction temperature and the Cl_2 molar ratio. Figure 3f clearly shows that the conversion of SrO into $SrCl_2$ occurs even at low Cl_2 molar ratio and high temperatures, indicating high selectivity for Sr in the presence of MgO. In summary, it is clear from the calculation results that reacting at a low temperature is beneficial for achieving high selectivity for Sr when it exists in the SrO form in concrete waste.

Identical calculations were repeated for $SrCO_3$ with CaO, $CaCO_3$, and MgO, and these results are shown in Fig. 4. Interestingly, an increase in the reaction temperature resulted in an increase in the $SrCl_2/CaCl_2$ ratio in the $SrCO_3$–CaO system (Fig. 4a). It is clearly shown in Fig. 4b that the $SrCl_2$ molar ratio increases with an increase in the reaction temperature. These results indicate that thermodynamic preference for the chlorination reaction moves from CaO to $SrCO_3$ with an increase in the reaction temperature. The opposite behavior was observed with the $SrCO_3$-$CaCO_3$ system shown in Fig. 4c, d. The $SrCl_2/CaCl_2$ ratio rapidly dropped with an increase in the reaction temperature, especially in the low temperature region. It is important to note that the effect of the Cl_2 molar ratio was negligible in Fig. 4c, whereas the $SrCl_2$ molar ratio increased linearly with an increase in the Cl_2 molar ratio (Fig. 4d). This result means that an increase in the Cl_2 molar ratio produces both $SrCl_2$ and $CaCl_2$ at an identical ratio, which is dependent only on the reaction temperature. High $SrCl_2/MgCl_2$ values were identified in the $SrCO_3$–MgO system (Fig. 4e) regardless of the reaction temperature. The effect of the reaction temperature on the $SrCl_2$ molar ratio was not distinguishable, as shown in Fig. 4f, indicating that $SrCO_3$ may react with chlorine prior to MgO under any of the conditions considered in this work. The calculation results with $SrCO_3$ suggest that operation at a high temperature is beneficial, except for the $SrCO_3$–$CaCO_3$ system, in order to ensure a high $SrCl_2/CaCl_2$ ratio. Recalling that a high $SrCl_2/CaCl_2$ ratio was observed at low temperatures with SrO, it can be summarized that the optimum reaction temperature may vary according to the chemical forms of Sr and Ca.

The effects of the reaction temperature and duration on the chlorination reaction of SrO were investigated and the results are shown in Fig. 5. The conversion ratio on the *y*-axis indicates the ratio of SrO converted to $SrCl_2$ (and Sr_4OCl_6) relative to the initial amount of SrO, which was calculated using the equation below,

$$\text{Conversion ratio} = \left(w_f - w_0\right)/\left(w_0 \times \left(MW_{SrO}/MW_{SrCl2}\right)\right) \quad (1)$$

where w_f is the weight measured after reaction, w_0 is the initial weight, MW_{SrO} is the molecular weight of SrO (= 103.62 g/mol), and MW_{SrCl2} is the molecular weight of $SrCl_2$ (= 158.53 g/mol). It is clear in the figure that the conversion ratio increases with an increase in the reaction time. It is interesting to observe that the maximum conversion ratio values were less than 0.4 in the reaction temperature range of 300–600 °C. This result may stem from the limited diffusion of chlorine within the solid phase at this temperature range. The conversion ratios at this temperature range require additional investigations. After 4 h of reaction, the conversion ratio increased from 0.155 to 0.320 when the temperature increased from 300 to 400 °C. When the temperature was increased further to 500 °C, the conversion ratio dropped profoundly to 0.0966 and then returned to 0.350 at 600 °C. This trend was confirmed by repeated experiments to ensure that it was not a result of any experimental errors. The reason for the poor conversion ratio at 500 °C is not clear at this point; however, it is obvious that the chlorination reaction should be conducted at or above 700 °C to achieve a high conversion ratio with SrO. These results eliminate the feasibility of a low-temperature operation for the high $SrCl_2/CaCl_2$ ratio proposed in the thermodynamic calculations with SrO (Fig. 3). Based on the outcomes of this work and previous documents [9, 10], it is obvious that the conversion of CaO and $CaCO_3$ into $CaCl_2$ during the chlorination reaction of SrO is not avoidable. Here it should be noted that the highest reaction temperature was limited to 800 °C, below melting point of $SrCl_2$, 874 °C, in order to avoid volatilization of the reaction product. As the conversion ratio is derived from weight change, volatilization of $SrCl_2$ results in reduced conversion ratio. After repeated experiments, the quartz reactor was clean and high conversion ratio of 0.914 was observed after reaction at 800 °C for 3 h.

Structural changes upon the chlorination reactions were investigated. Figure 6a shows the XRD measurement results of the samples reacted at 300 °C. The formation of the $SrCl_2$

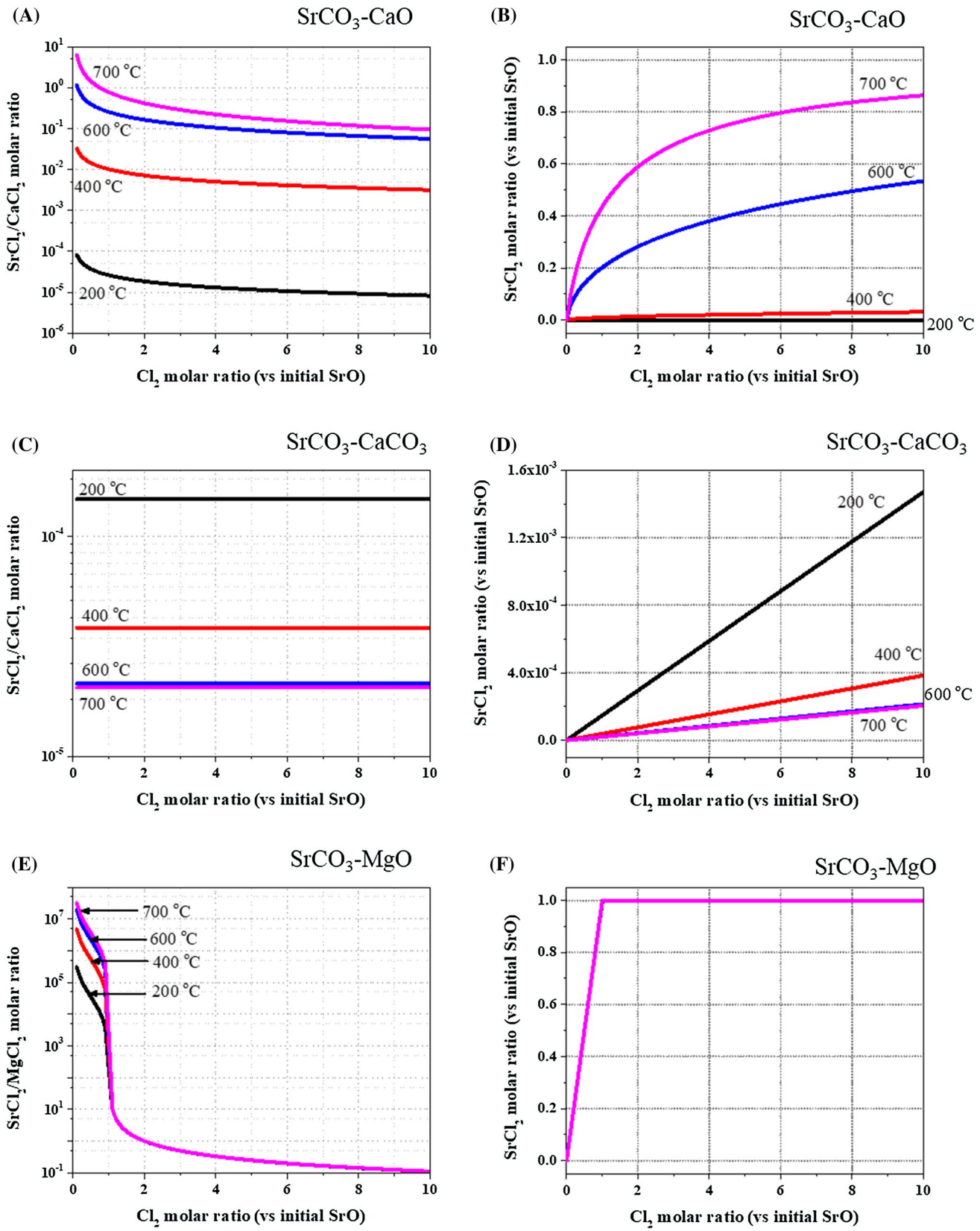

Fig. 4 Equilibrium compositions (**a**, **c**, **e**) and conversion ratios of $SrCl_2$ (**b**, **d**, **f**) of the $SrCO_3$–CaO (**a**, **b**), $SrCO_3$–$CaCO_3$ (**c**, **d**), and $SrCO_3$–MgO (**e**, **f**) systems at various temperatures and Cl_2 molar ratios with an initial $SrCO_3$ concentration of 1 ppm versus CaO, $CaCO_3$, or MgO

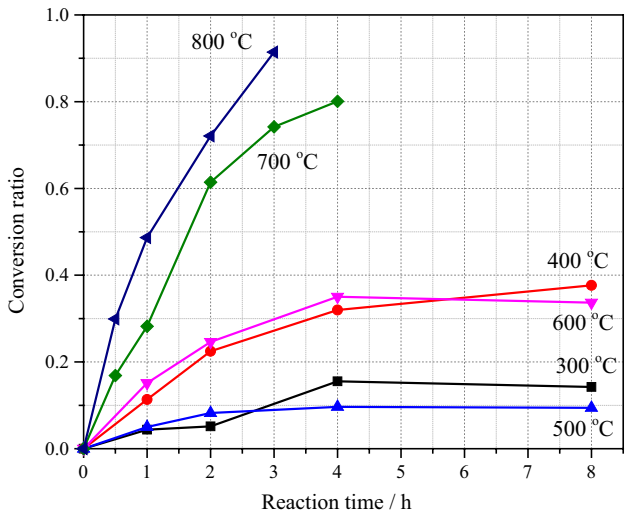

Fig. 5 Conversion ratio of SrO as a function of both the reaction temperature and the time

phase (JCPDS #01-072-1537) was confirmed from the XRD peaks without any other phases. It was identical in the samples reacted at 400 °C, as shown in Fig. 6b. It is clear in the figures that the relative intensity of the $SrCl_2$ peaks increases with an increase in the conversion ratio. When the reaction temperature increased to 500 °C, along with $SrCl_2$, a new phase of Sr_4OCl_6 (JCPDS #01-086-1832) was identified regardless of the reaction time, as shown in Fig. 6c [16, 17]. These results suggest that the sudden decrease in the conversion ratio at 500 °C is related to the formation of Sr_4OCl_6, though additional experiments are necessary to explain the details of the relationship. A thermodynamic analysis of the formation of Sr_4OCl_6 was not available due to lack of data in the HSC chemistry code. The trend was similar in the 600 and 700 °C cases, which exhibited peaks of SrO (JCPDS #01-075-6979), $SrCl_2$, and Sr_4OCl_6, as shown in Fig. 6d, e. It was interesting to observe the outcome at 800 °C (Fig. 6f). After 0.5 and 1 h of the reaction, tiny peaks of Sr_4OCl_6 were observed with high intensities of $SrCl_2$ and SrO peaks. When the reaction time was increased to 2 h, the peaks of $SrCl_2$ are dominant while those of SrO are relatively small. At the same time, the peaks of Sr_4OCl_6 disappeared, suggesting that this phase was converted into $SrCl_2$ at 800 °C by the chlorination reaction. At this temperature, thermal decomposition of Sr_4OCl_6 into SrO and $3SrCl_2$ might be negligible due to its high thermal stability [17]. After 3 h of the reaction, only $SrCl_2$ peaks were observed, suggesting that the amount of SrO is below the detection limit of the XRD measurement technique. These XRD measurement results show that the reaction product generated via the chlorination reaction changes with the reaction temperature and time only at 800 °C. It should be noted here that the presence of Sr_4OCl_6 does not affect the conversion ratio results shown in Fig. 5, because its weight is identical to $SrO–3SrCl_2$. Therefore, the conversion ratio still represents the amount of SrO reacted with Cl_2 when the reaction products are $SrCl_2$ and Sr_4OCl_6. However, it is possible that other chlorides or oyxchlorides have been produced during the experiments, which are not detectable by the XRD measurements.

The thermodynamic calculation results suggested that the Ca compounds react with chlorine gas to produce $CaCl_2$ during the chlorination of SrO. A set of experiments was conducted in order to identify the chlorination reaction behavior of CaO and $CaCO_3$. Figure 7 shows the effect of the reaction temperature on the conversion ratio after 4 h of the reaction under a 96 mL/min Ar + 4 mL/min Cl_2 flow. The chlorination reaction behavior of $SrCO_3$ was also investigated under identical conditions. Here, $Ca(OH)_2$ was not included due to its decomposition temperature of 512 °C and experimental confirmation of partial decomposition at 300 and 400 °C. It is clearly shown in the figure that CaO has higher conversion ratios than those of SrO, except at 800 °C. The conversion ratio of CaO peaked at 600 and 700 °C and then decreased slightly at 800 °C. This result may have come from evaporation of $CaCl_2$ (melting point 775 °C) or the temperature dependence of the chlorination reaction. In contrast, the chlorination reaction of $CaCO_3$ began at 700 °C with a conversion value of 0.361, which is only 38.7% of the conversion ratio of CaO at 700 °C. The chlorination reaction began at 300 °C in $SrCO_3$, and the conversion ratio dramatically increased to 0.424 and 0.806 at 400 and 500 °C, respectivley. However, the conversion ratio decreased with a further increased in the reaction temperature to 600 and 700 °C. It is interesting to note that SrO exhibited an especially low conversion ratio value at 500 °C, where the highest conversion value was observed with $SrCO_3$. These results suggest that the high selectivity for SrO estimated in the thermodynamic calculations is not readily achievable in the presence of CaO. In addition, it is recommended to operate the chlorination decontamination process at or above 700 °C.

Conclusions

A chlorination technique was introduced for use during the decontamination of ^{90}Sr-contaminated concrete waste. Thermodynamic investigations suggested that the chlorination technique is a promising approach to convert SrO into $SrCl_2$ with relatively low conversion ratios in Ca compounds and MgO. However, the experimental results revealed that the reaction temperature should be at least 700 °C to achieve a significant amount of $SrCl_2$ and that CaO exhibited higher or similar conversion ratios compared to those of SrO. In conclusion, the proposed chlorination decontamination technique has the merits of a simple process stream for Sr removal, while the simultaneous

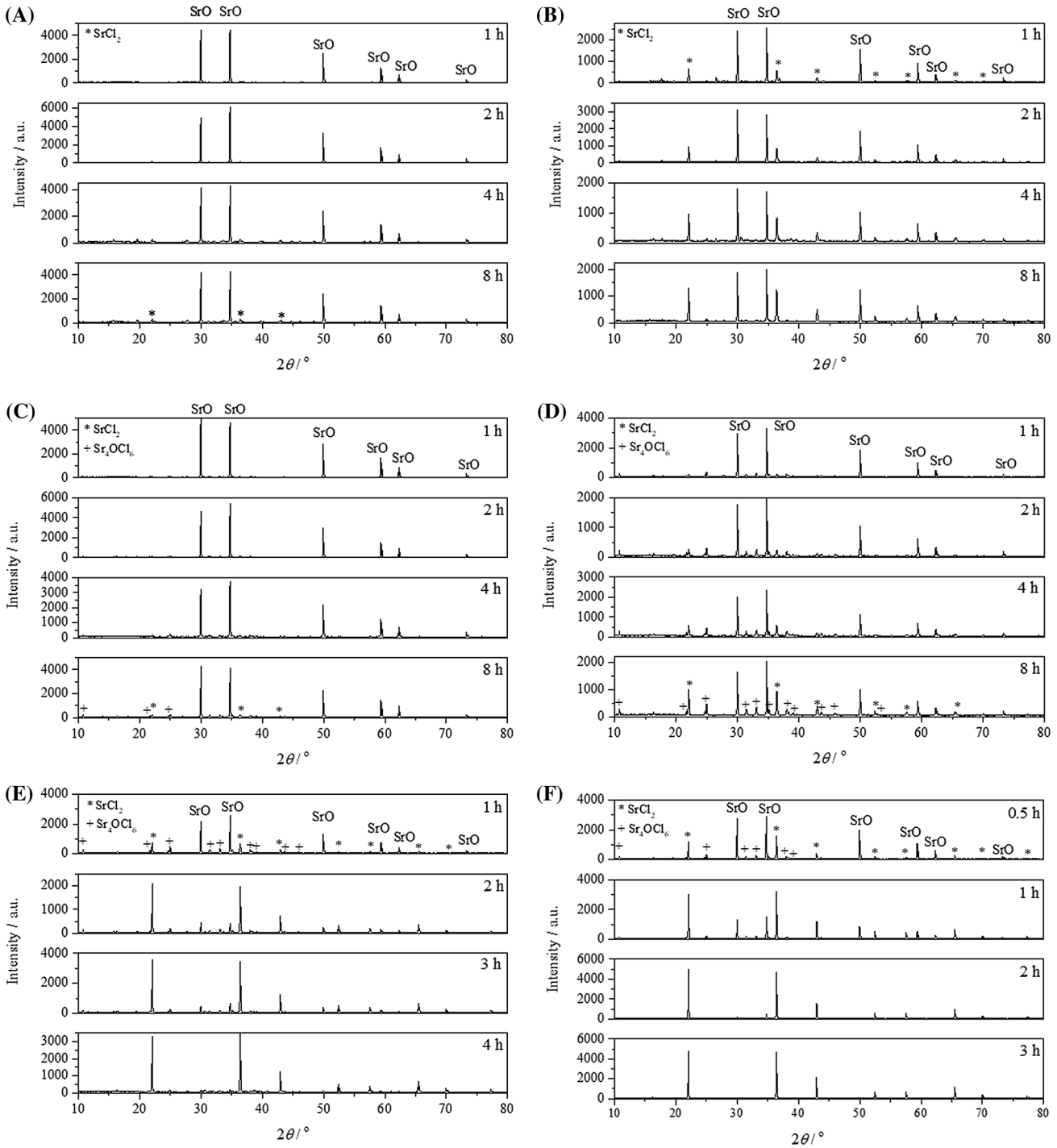

Fig. 6 XRD measurement results as a function of both the reaction temperature, at **a** 300, **b** 400, **c** 500, **d** 600, **e** 700, and **f** 800 °C, and the reaction time at each temperature

removal of non-radioactive Ca may lessen its decontamination factor. In addition, further investigations including interactions between chlorides and volatilization of chlorides might be necessary before applying the chlorination technique to the decontamination of concrete waste.

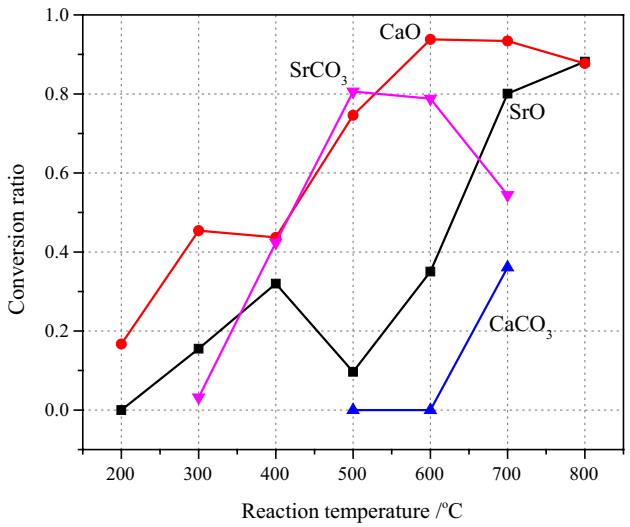

Fig. 7 Conversion ratio values of SrO, $SrCO_3$ CaO, and $CaCO_3$ as a function of the reaction temperature after 4 h of the reaction with a 96 mL/min Ar + 4 mL/min Cl_2 flow

Acknowledgements This research was funded by the Nuclear R&D program of the Korean Ministry of Science and ICT (2017M2A8A5015147).

References

1. Bilici S, Kulahci BA (2019) Spatial modelling of Cs-137 and Sr-90 fallout after the Fukushima nuclear power plant accident. J Radioanal Nucl Chem 322:431–454
2. United States Environmental Protection Agency. Radionuclide basics: Strontium-90. https://www.epa.gov/radiation/radionuclide-basics-strontium-90
3. International Atomic Energy Agency (2001) Methods for the minimization of radioactive waste from decontamination and decommissioning of nuclear facilities. Technical Report Series No. 401, IAEA, Vienna
4. Cheremisina O, Sergeev V, Alabusheva V, Fedorov A, Iliyna A (2018) The efficiency of strontium-90 desorption using iron(III) solutions in the decontamination process of radioactive soils. J Ecolog Eng 19:149–153
5. Hasdemir S, Tugrul A, Yilmaz M (2016) The effect of natural sand composition on concrete strength. Constr Build Mater 112:940–948
6. Kosmatka SH, Wilson ML (2011) Design and control of concrete mixtures (15th Edition). Portland Cement Association. ISBN 0-89312-272-6
7. Lee KY, Oh M, Kim J, Lee EH, Kim IS, Kim KW, Chung DY, Seo BK (2018) Trends in technology development for the treatment of radioactive concrete waste. J Nucl Fuel Cycle Waste Technol 16:93–105
8. Nuclear Energy Agency (2011) The NEA co-operative programme on decommissioning, decontamination and demolition of concrete structures. NEA/RWM/R(2011)1, Boulogne-Billancourt
9. Yake DE, Ulrichson DL (1981) Kinetics of calcium oxide chlorination and pore closure models. Chem Eng Commun 12:97–120
10. Orosco P, Barrios O, Ojeda M (2019) Extraction of potassium from microcline by chlorination. Minerals 9:295
11. HSC chemistry software, Outotec, Pori, Finland
12. Christahl M, Anton S (1984) The thermal properties of group II metal hydroxide and of the octa-hydrates of strontium and barium hydroxide. Int J Hydrog Energy 9:603–607
13. Kleykamp H (1985) The chemical state of the fission products in oxide fuels. J Nucl Mater 131:221–246
14. Arvanitidis I, Sichen DU, Sohn HY, Seetharaman S (1997) The intrinsic thermal decomposition kinetics of $SrCO_3$ by a nonisothermal technique. Metall Mater Trans B 28B:1063–1068
15. Karunadasa KSP, Manoratne CH, Pitawala HMTGA, Rajapakse RMG (2019) Thermal decomposition of calcium carbonate (calcite polymorph) as examined by in-situ high-temperature X-ray powder diffraction. J Phys Chem Solids 134:21–28
16. Hagemann H, Kubel F, Bill H (1996) Crystal structure of Sr_4OCl_6. Eur J Solid State Inorg Chem 33:1101–1109
17. Gwak SJ, Arunkumar P, Im WB (2014) A new blue-emitting oxohalide phosphor $Sr_4OCl_6:Eu^{2+}$ for thermally stable, efficient white-light-emitting devices under near-UV. J Phyc Chem C 118:2686–2692